23rd Applied Aerodynamics Conference, June 6-9 2005, Toronto, Canada

Grid Resolution Study of a Drag Prediction Workshop Configuration Using the NSU3D Unstructured Mesh Solver

Dimitri J. Mavriplis *

Department of Mechanical Engineering, University of Wyoming, Laramie WY 82071, USA

A grid convergence and sensitivity study is carried out on a wing-body configuration which was the subject of the second AIAA drag prediction workshop held in 2003. Sensitivity of the computed force coefficients to the formulation of the viscous terms, the distance function evaluation, and the levels of artificial dissipation are investigated, as well as the behavior of these effects on grids of very high resolution. For a given family of grids, grid convergence is demonstrated for drag coefficient values on a family of self-similar meshes using up to 72 million grid points. However, on a mesh of 65 million points using similar resolution but different topologies near the trailing edge region, substantially different results are obtained. The results indicate that sensitivity to discretization errors is dominant over sensitivity to the particular modeling errors considered in this study, and that effects such as spanwise grid stretching may have substantial repercussions on overall simulation accuracy even at very high levels of resolution.

I. Introduction

Over the last four years, the AIAA Applied Aerodynamics Committee has sponsored two Drag Prediction Workshops (DPW), with the aim of assessing the state of the art of current Computational Fluid Dynamics (CFD) solvers at predicting absolute and incremental drag changes on generic transonic transport aircraft configurations. The results of the first workshop[1] revealed relatively large scatter between submitted participant calculations using a wide range of codes. The results of the second workshop[2] demonstrated substantially reduced scatter, but still much higher levels than generally desirable. Furthermore, with several notable exceptions, the bulk of the computational results in both workshops demonstrated relatively poor agreement with experiment, especially in terms of lift versus incidence, and moment prediction.

Although the configurations chosen for the two workshops consist of relatively simple wing-body and wing-body-nacelle-pylon geometries, which are the basis for many industrial CFD calculations, the flow fields at the test conditions of interest are now known to contain substantial regions of separated flow, and are generally considered to be representative of off-design conditions. In a typical design study, once such regions of separated flow are discovered, the geometry would be modified until these regions are removed or at least minimized, producing a cleaner cruise configuration. Generally, for cases with minimal amounts of separated flow, state-of-the-art Reynolds averaged Navier-Stokes (RANS) solvers can be used with a high degree of confidence. However, the numerical prediction of force and moment coefficients for off-design conditions and for flows with substantial amounts of separation represents a difficult task which is currently

*Professor, Department of Mechanical Engineering, University of Wyoming, AIAA Associate Fellow.

a pacing item, as demonstrated by the wide scatter and poor agreement with experimental data in the two workshops.

In assessing the predictive ability of various simulation codes on these problems, the various sources of error must be considered, including discretization error, modeling error, and even experimental errors, both in the data acquisition and reduction/correction process. In previous work,[3,4] a quantification of discretization and modeling error was attempted by computing the first and second drag workshop cases with several structured and unstructured mesh solvers on a sequence of coarse and fine meshes. These two studies revealed similarly surprising trends: a notably wide scatter of predicted drag values between the various codes, and a seemingly lack of grid convergence as represented by a widening of the scatter between code results with increasingly finer grids. The second study was confined to comparing three unstructured mesh solvers on similar grids for the second drag workshop configurations, and identified a number of possible reasons for discrepancies between the various codes, such as the use of cell or vertex based discretizations, the use of wall functions, the use of prismatic or tetrahedral elements in boundary layer regions, different approaches for calculating the distance function required by the turbulence model, the use of thin layer versus full Navier-Stokes terms, and the use of upwind versus artificial dissipation based schemes. The fact that the results of the various codes do not converge to each other as the grid is refined suggests either that the various codes contain different modeling errors, and/or that the grids used in the refinement study were not fine enough to situate the results in the asymptotic region of convergence of the spatial discretization error of the solvers. The current work represents an attempt to further pursue quantification of these errors with one particular unstructured mesh solver used in the previous study. In order to assess the influence of various modeling errors, the sensitivity of the computed solution to changes in various discretization strategies is examined, and a more extensive grid convergence study is undertaken, using grids containing up to 72 million vertices, which represents an order of magnitude more grid points than the grids used in the original workshop.

II. DLR-F6 Configuration

The DLR-F6 configuration was the basis for the second AIAA drag prediction workshop.[2] The DLR-F6 represents a twin-engine wide-body aircraft which has been the subject of various experimental and computational studies. Multiple engine geometries and installation locations have been tested and computed numerically,[5] although only one engine and installation configuration was studied in the drag workshop. The current study is restricted to the simple wing-body geometry of the DLR-F6, in the absence of any nacelle and pylon. The wing aspect ratio is 9.5, and the leading edge sweep is 27.1 degrees. The design cruise condition for this configuration consists of a freestream Mach number of 0.75, a Reynolds number based on the mean aerodynamic chord of 3 million, and a fixed lift coefficient of 0.5. As opposed to the drag workshop conditions, which were run at fixed C_L (by varying the incidence), the current calculations were performed at a fixed incidence of 0 degrees, and the resulting lift and drag coefficients are examined as a function of the grid resolution and other modeling variables, since this corresponds to the more traditional approach for examining grid convergence.

III. NSU3D Solver

The NSU3D code is an unstructured mesh multigrid Reynolds-averaged Navier-Stokes (RANS) solver for high Reynolds number external aerodynamic applications. Solutions using NSU3D were submitted for the first and second drag prediction workshops, and follow-on studies comparing NSU3D with other structured and unstructured solvers for the drag workshop cases have been performed[6,7,3,4]

The NSU3D discretization employs a vertex-based approach, where the unknown fluid and turbulence variables are stored at the vertices of the mesh, and fluxes are computed on faces delimiting dual control volumes, with each dual face being associated with a mesh edge. This discretization operates on hybrid

mixed element meshes, generally employing prismatic elements in highly stretched boundary layer regions, and tetrahedral elements in isotropic regions of the mesh away from the aircraft surfaces. A single edge-based data-structure is used to compute flux balances across all types of elements. The convective terms are discretized as central differences with added matrix dissipation. Second-order accuracy is achieved by formulating these dissipative terms as an undivided bi-harmonic operator, which is constructed in two passes of a nearest neighbor Laplacian operator. In the matrix form, this dissipation is similar to that produced by a Riemann solver gradient-based reconstruction scheme, and is obtained by replacing the difference in the reconstructed states on each side of the control volume interface by the undivided differences along mesh edges resulting from the biharmonic operator construction. These differences are then multiplied by the characteristic matrix to obtain the final dissipation terms.

The baseline NSU3D discretization employs a finite-difference scheme to approximate the thin-layer form of the viscous terms for the Navier-Stokes equations, although this is done in a multidimensional fashion, by computing a Laplacian of the velocity field.[8] The main approximation in this approach is the omission of the cross-derivative viscous terms, and the assumption of a locally constant viscosity. The discretization of the full Navier-Stokes terms has also been implemented. This is achieved by first computing gradients of the flow variables at the grid vertices, using an edge-based loop, and then using a second edge loop to assemble the viscous flux balance at each vertex, based on these gradients. This approach results in an extended neighbor-of-neighbor stencil, which is less accurate than a nearest neighbor stencil. However, a nearest neighbor stencil discretization of second derivatives on mixed element meshes requires the use of a cell data-structure, while the current approach relies exclusively on the edge-data structure. In order to improve the accuracy and stability of this discretization, a hybrid approach is adopted, where the second derivatives in the directions aligned with the incident mesh edges are computed using a nearest neighbor stencil on the edges, while the remaining terms are computed using the extended stencil using the two pass approach.

The basic time stepping scheme in NSU3D consists of a three stage explicit multistage scheme. Convergence is accelerated by a local block-Jacobi preconditioner in regions of isotropic grid cells. In boundary layer regions, where the grid is highly stretched, a line preconditioner is employed to relieve the stiffness associated with the mesh anisotropy.[9] An agglomeration multigrid algorithm is used to further enhance convergence to steady-state.[8,10] The Jacobi and line preconditioners are used to drive the various levels of the multigrid sequence, resulting in a rapidly converging solution technique. Figure 1(a) illustrates a typical convergence history for the DLR-F6 configuration at Mach=0.75, 0 degrees incidence, and 3 million Reynolds number, for the 3.0 million point grid described below. The solver is generally run 500 multigrid cycles, and up to 1000 cycles for more stringent cases with larger amounts of separated flow. On 16 AMD Opteron 242 processors, 500 multigrid cycles on the 3.0 million point grid requires approximately 2.5 hours of wall clock time. On 128 cpus of the NASA Columbia system (SGI Altix), this case requires 10 minutes of wall clock time. The finest meshes described below contain 65 million and 72 million grid points. The availability of the NASA Columbia Supercomputer enables rapid turnaround for solutions on these fine grids. For example, on 128 cpus, the 72 million point grid required approximately 4.5 hours of cpu time to produce a converged solution. Figure 1(b) illustrates the scalability obtained on the NASA Columbia supercomputer for the 72 million point grid, going from 128 cpus to 2008 cpus, demonstrating slightly superlinear speedup. A computational rate of approximately 3 Tflops was obtained on 2008 cpus, using 5 multigrid levels. Using up to 6 multigrid levels reduces modestly the scalability and computational rates at high processor counts due to the increased amount of communication required on the coarse grid levels, but generally results in fastest overall convergence. On 2008 cpus, a solution on the 72 million point grid could be obtained in 20 minutes of wall clock time (2 seconds per multigrid cycle).

IV. Computational Grids

A half-span model of the DLR-F6 wing-body geometry was used in the current study, using a symmetry plane boundary condition along the fuselage centerline, since all conditions involve zero sideslip. A total of

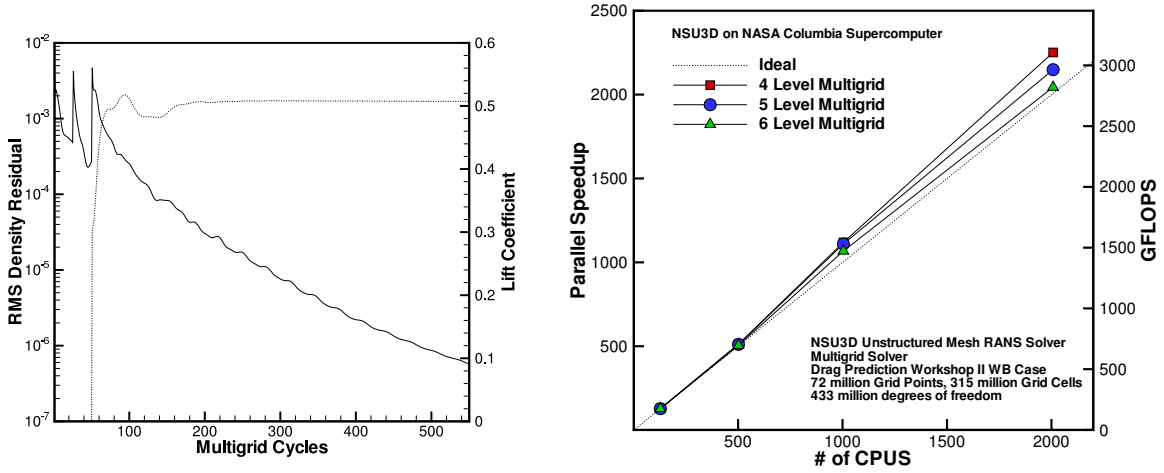

(a) (b)

Figure 1. (a): Multigrid Convergence Rate using 5 grid levels for NSU3D Solution of Viscous Turbulent Flow over Aircraft Configuration on intermediate 3.0M pt mesh. (b): Scalability and Computational Rates Achieved on NASA Columbia Supercomputer for NSU3D on 72M pt mesh illustrating the effect of various multigrid levels on overall scalability.

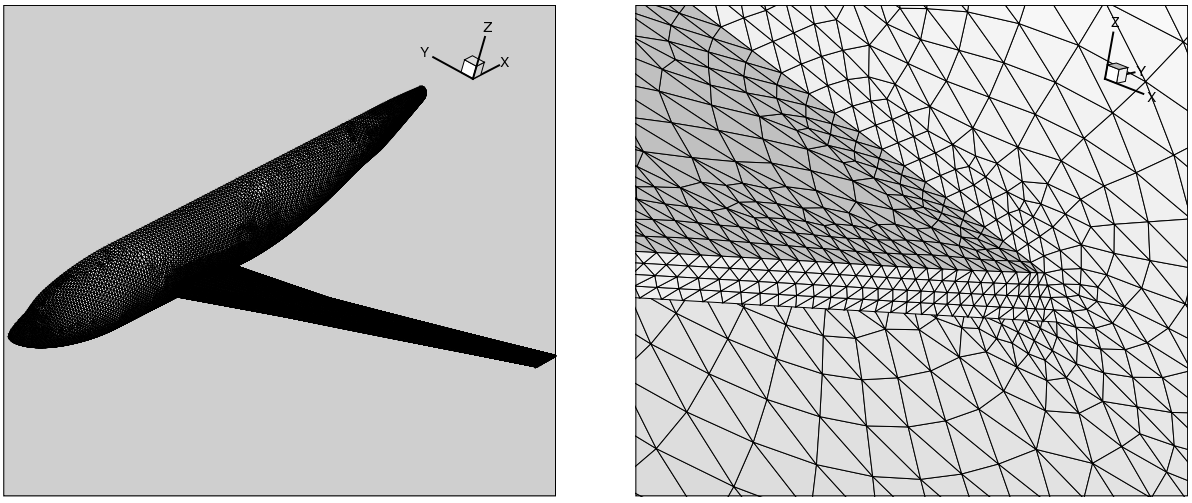

(a) (b)

Figure 2. (a): Illustration of medium resolution (3.0 million pt) mesh about DLR-F6 wing-body configuration and (b) closeup showing resolution in wing root trailing edge fuselage junction.

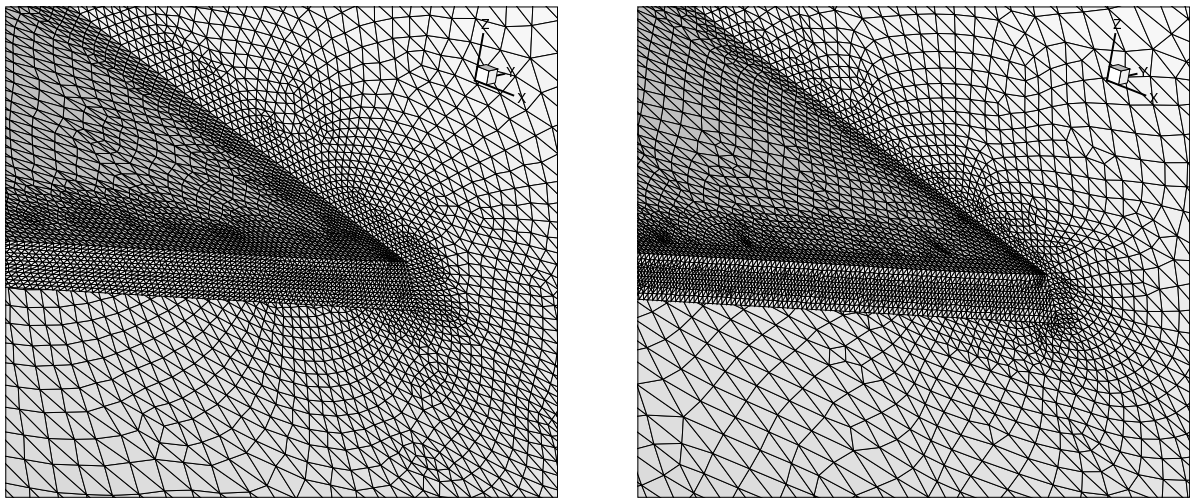

(a) (b)

Figure 3. Comparison between surface resolution for 72 million point grid (a) and 65 million point grid (b) in wing root fuselage junction region.

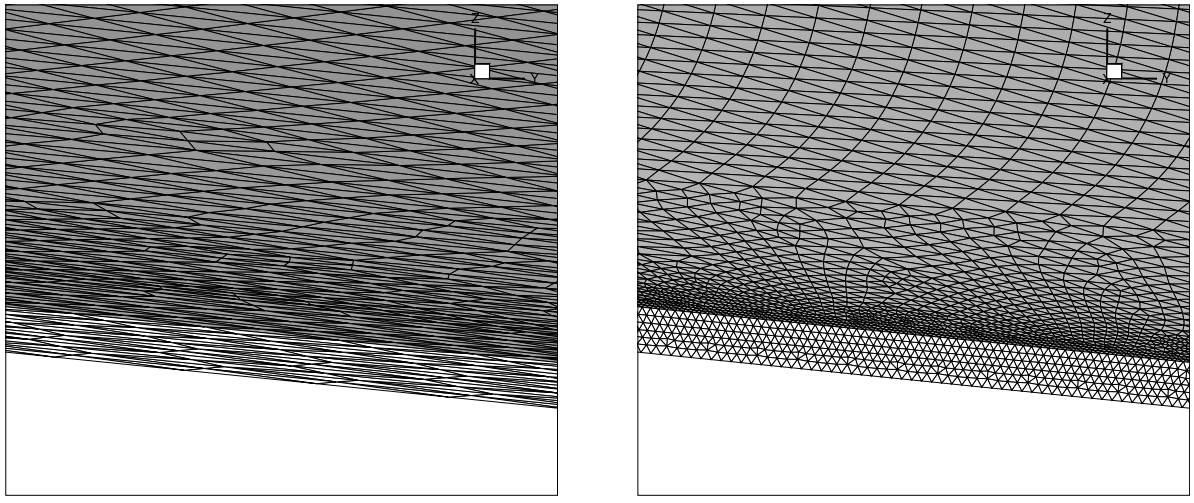

(a) (b)

Figure 4. Comparison between surface resolution for 72 million point grid (a) and 65 million point grid (b) in trailing edge region in the vicinity of 60% span region illustrating spanwise stretching for the 72 million point grid.

five different grids are used in the current study. The first three meshes contain 1.12 million, 3.0 million, and 9.13 million vertices. Two finer meshes containing 72 million points and 65 million points were also generated and used in the grid refinement studies. The first three grids were generated at NASA Langley using the VGRIDns grid generation package,[11] and supplied as official grids for the second drag workshop, and are available at the workshop website.[12] A detailed description of these grids is given in reference.[4] The 3.0 million point grid constitutes a "best-practices" medium resolution type grid for a wing-body configuration and is depicted in Figure 2. This grid contains a total of 55,069 points on the aircraft surface (no-slip condition). The maximum chordwise grid spacing at the wing leading edge was approximately 0.45% local chord and the maximum chordwise spacing at the trailing edge was approximately 0.33% of the local chord. A total of four cells were used across the blunt trailing edge. The maximum chordwise spacing at the root and crank is approximately 2.7% of chord, and 1.7% at the tip. Spanwise stretching was used along the leading and trailing edges to reduce the overall number of grid points, resulting in a maximum spanwise aspect ratio of approximately 20 to 1 in these regions. However, there is no spanwise stretching in the root and tip regions of the wing, as can be seen in the closeup of Figure 2(b). A wall normal spacing of 7.0e-06 of the mean aerodynamic chord was used in order to achieve a value of $y^+ = 1$ for the grid points closest to the wall, which also yielded approximately 26 cells in the boundary layer region.

The 1.12 million point and 9.13 million point grids were generated as a global coarsening and refinement, respectively, of the medium 3.0 million point grid, in order to create a family of coarse and fine grids with similar relative spacings and topologies, for use in a grid refinement study. This is achieved using the same local spacing parameters in the VGRIDns grid generation process, but using different values of the global spacing parameter, and different values of the minimum wall spacing parameter.[4]

In keeping with this family of grids concept for grid convergence studies, a finer grid was generated by subdividing each cell in the 9.13 million point grid into eight self similar finer cells, thus increasing the global grid resolution by a factor of 8, and resulting in 72 million grid points. In this refinement, the newly created surface points are positioned using linear interpolation based on the existing coarse grid points, and are not repositioned on the original CAD surface of the geometry, although at this level of resolution, these differences can be expected to be small. These four meshes form a single "family" of meshes, as they are all derived from the same specification of "relative" surface grid spacings. Another fine mesh consisting of 65 million grid points was generated at NASA Langley using the VGRIDns package. Although this mesh contains similar overall spacings to the 72 million grid point mesh described above, it is not derived from any of the other meshes described above. Figures 3 and 4 provide an illustrative comparison of the these two fine meshes in the trailing edge region of the wing. Both meshes exhibit similar resolution in the wing root region (c.f. Figure 3), with the 72 million point mesh containing 12 cells across the blunt trailing edge, and the 65 million point mesh containing 8 cells across the blunt trailing edge. However, in the midspan region, the mesh topologies are substantially different, with strong spanwise stretching evident in the 72 million point mesh (c.f. Figure 4), while the 65 million point mesh uses added spanwise resolution to maintain isotropic cells in the vicinity of the trailing edge. However, the 72 million point mesh still contains twice the chordwise resolution across the blunt trailing edge compared to the 65 million point mesh in these regions (12 cells versus 6 cells). Nevertheless, the 65 million point mesh overall contains roughly twice the number of points on the entire aircraft surface compared to the 72 million point mesh, largely due to the added spanwise resolution, as shown in Table 1.

In all cases, the fully tetrahedral meshes generated by the VGRIDns process are converted to mixed prismatic-tetrahedral cell meshes, with a small number of pyramidal elements used to stitch together regions of prismatic and tetrahedral interfaces. This has no effect on the number of vertices and thus the overall number of degrees of freedom in the computation, although the number of edge-based fluxes is reduced, thus lowering the overall computational expense. The numbers of cells and points of the various grids used in this study are summarized in Table 1.

Table 1. Characteristics of Meshes used in Grid Refinement Study.

Grid Points	Tetrahedra	Prisms	Pyramids	Points on Aircraft Surface	Cells Across TE
72183630	258251288	57062312	160524	474926	12
65402804	278970020	35143326	0	976828	6 - 8
9146678	32268034	7132789	26754	118903	6
3017614	10012851	2543191	14697	55069	4
1125520	3046727	1172066	8464	25104	2

V. Overall strategy

The current study aims to assess the sensitivity of the solution process to modeling and discretization error. With respect to modeling error, the most obvious source is the modeling of turbulence and transition. However, these are not considered in the current study, and all cases are run using the Spalart-Allmaras one equation turbulence model[13] in fully turbulent mode. The overall goal is not the development of a "best" simulation procedure, but rather a careful assessment of the discretization error and other modeling errors, and thus fixing the turbulence and transition models is a pre-requisite for being able to best examine these other errors sources.

The sensitivity of the solution with respect to the modeling of the viscous terms is examined by computing on the same grid the solution using the multi-dimensional thin-layer approximation of the Navier-Stokes equations as employed by the baseline NSU3D solver, and the extended stencil discretization of the full Navier-Stokes terms. The multi-dimensional thin-layer approximation used in NSU3D is appealing because it is easily constructed as a nearest neighbor stencil using a loop over the mesh edges, and is particularly robust, while the full Navier-Stokes terms require additional computational resources and result in slower convergence due to the use of an extended stencil.

The Spalart-Allmaras turbulence model requires knowledge of the distance to the nearest wall for each field grid point. This computation of this quantity has proved to be somewhat resource intensive, and also prone to error. In fact, small differences are known to exist between the results generated by various approaches to solving this problem on the same grid. The resulting distance function is not necessarily smooth, as the location of the closest surface can change discontinuously as one proceeds outwards in a concave region of the geometry, for example. This in turn implies that the accuracy of the computed distance may not scale with grid resolution in the same manner as the overall discretization error and may contribute to anomalies in a grid convergence study. To this effect, we study the sensitivity of the solution to various approaches for computing the distance function, including an exhaustive search procedure, generally acknowledged to produce the most "exact" values, but perhaps involving non-smooth variations in the distance function, and two partial-differential-equation-based methods. The first approach involves the solution of the Eikonal equation,[14] while the second approach involves the solution of a Poisson equation.[15] While the first approach has been shown to produce distance function values which are more closely related to those produced by the exhaustive search method, the results are known to be only first order accurate in space. The Poisson equation approach, on the other hand, produces distance values which deviate substantially from the exhaustive search values at large distances away from the wall, but are close to these values in near wall regions, and exhibit second-order discretization error. The Poisson equation approach is also the fastest distance function calculation method, since it can easily be parallelized and solved using the same multigrid approach used for the flow equations, while the Eikonal equation is solved with a sweeping approach, which is difficult to parallelize, and is currently implemented as a preprocessing step running on a single processor. Both these approaches are more than an order of magnitude faster than the exhaustive search method, and remain practical for very large mesh resolutions, where the cost of the exhaustive search approach becomes prohibitive.

The sensitivity of the solution to the levels of artificial dissipation is also examined by recomputing the solutions on the same grid at the same conditions with the value of the artificial dissipation parameter being half its nominal value. Finally, the above calculations are performed on the full sequence of coarse and fine meshes.

VI. Results

A. Distance Function Sensitivity

The lift and drag values computed on the 1M point, 3M point, and 9M point grids using the three different distance function evaluation methods are given in Table 2, for the transonic flow conditions of Mach=0.75, and 0^o incidence. In all cases, the values obtained using the Eikonal equation approach are almost indistinguishable from those obtained with the exhaustive search method. For example, there is always substantially less than 1 count difference in the computed drag between these methods. The computed lift values are consistent to three significant figures, with the smaller differences observed on finer grids. The Poisson equation approach produces more discrepancies in the computed force coefficients, showing variations of 2.8 counts of drag and approximately 1% difference in the computed lift coefficient on the coarsest mesh, although these differences are reduced on the finer grid. Overall, the Eikonal equation approach is the preferred method, since it differs very little from the exhaustive search approach, but is over an order of magnitude faster in computing the distance function. On the other hand, this method is difficult to parallelize since it relies on a sweeping algorithm, and is currently implemented as a sequential preprocessing step. This approach has been used to compute the distance function for the 65M point grid, requiring approximately 100 minutes on a single Itanium processor of the NASA Columbia machine (SGI Altix system). The distance function for the 72M point grid was obtained by interpolating the distance function computed using the exhaustive search method on the coarser 9M point grid, since this grid is obtained through a subdivision process applied to the 9M point grid.

Table 2. Computed Lift and Drag Coefficients at Mach=0.75, Incidence=0^0, on various grids using three different approaches for computing the distance function.

Grid Size	Distance Function	C_L	C_D
1M pts	Exhaustive Search	0.50546	0.03139
1M pts	Eikonal Equation	0.50563	0.03138
1M pts	Poisson Equation	0.49915	0.03111
3M pts	Exhaustive Search	0.50732	0.02942
3M pts	Eikonal Equation	0.50751	0.02942
3M pts	Poisson Equation	0.50452	0.02927
9M pts	Exhaustive Search	0.51410	0.02882
9M pts	Eikonal Equation	0.51404	0.02882

B. Full Navier-Stokes Terms

The flow field at the single condition of Mach=0.75 and 0 degrees incidence has been computed on the first three grids (1M, 3M, 9M points) using the original multi-dimensional thin-layer approximation in the baseline NSU3D code, and also using the edge-based implementation of the full Navier-Stokes terms, as described previously. The computed values of the force coefficients are given in Table 3 for all cases. In order to emphasize any differences due to the formulation of the viscous terms, these cases were run with reduced artificial dissipation levels, using half the nominal value of the artificial dissipation parameter, except on the

9M point grid, where the nominal value of was used, due to convergence problems with the lower dissipation levels.

In all cases, the differences between the values computed with the thin layer approximation and the full Navier-Stokes terms are minimal, corresponding to less than 2 counts of drag for the finer meshes of the sequence, and small variations in the third significant figure of the lift coefficient. For these cases, the multi-dimensional thin-layer assumption appears to be justified, and little change in the solution is observed in going to the full Navier-Stokes terms.

Table 3. Computed Lift and Drag Coefficients at Mach=0.75, Incidence=0^0, on various grids using the multi-dimensional thin-layer discretization and the extended stencil full Navier-Stokes discretization.

Grid Size	Viscous Terms	C_L	C_D	$CD_{Pressure}$	$CD_{Friction}$
1M pts	Thin Layer Approx.	0.5055	0.02960	0.01661	0.01298
1M pts	Full Navier Stokes	0.4960	0.02921	0.01652	0.01269
3M pts	Thin Layer Approx.	0.5012	0.02859	0.01568	0.01290
3M pts	Full Navier Stokes	0.5020	0.02841	0.01571	0.01270
9M pts	Thin Layer Approx.	0.5141	0.02882	0.01592	0.01290
9M pts	Full Navier Stokes	0.5154	0.02867	0.01594	0.01273

C. Grid Convergence Study and Sensitivity to Dissipation Levels

One of the principal goals of the current work is to study the behavior of the computed solutions as the grid is refined, in an attempt to demonstrate convergence of the spatial error with grid refinement. Theoretically, the NSU3D solver should exhibit second-order accuracy in space, meaning that a doubling of grid resolution should reduce the spatial error by a factor of 4. The most rigorous approach entails subdividing each cell of an existing coarser mesh into a finer mesh with 8 times the resolution, or half the relative grid spacing in all regions of the computational domain. This is the approach taken in the construction of the 72M point mesh, which was generated through subdivision of the 9M point mesh. The coarse 1M, 3M and 9M point meshes were generated using the VGRID generation package, but using the same relative grid spacing specifications, and can be expected to approximate a global grid refinement study. For a second-order accurate scheme, plotting the computed force coefficients as a function of the inverse of the square of the grid spacing, should produce a straight line curve. For a sequence of grids with similar relative spatially-varying grid resolutions, a common approach is to plot the computed force coefficients versus the number N of grid points to the -2/3 power,[3,4] where $N^{1/3}$ corresponds to some average grid spacing in three dimensions.

The sensitivity of the solution to the levels of artificial dissipation is included as part of the grid refinement study. Dissipation errors are often thought to be the dominant errors on coarser grids, and increasing the mesh resolution naturally leads to lower dissipation levels. However, the sensitivity of the solution to the prescribed levels of dissipation on any grid level can provide an indication of the level of dissipation errors on that grid level, and the sensitivity to dissipation levels can be expected to decrease for increasingly finer grids. The sensitivity to dissipation levels can also be used to estimate the magnitude of the effects of switching between an artificial dissipation scheme and an upwind scheme, or between various approximate Riemann solvers within an upwind scheme. The sensitivity to dissipation levels is obtained by comparing the results obtained using the nominal values of the dissipation scaling parameter, with the results obtained using half the nominal value. The nominal value has been determined empirically as a compromise between accuracy and robustness. The smaller value provides superior accuracy but may encounter convergence problems for finer grids at higher lift conditions.

Two conditions were considered for this study, the standard transonic condition of Mach=0.75, and 0 degrees incidence, and a subcritical case of Mach=0.3 and 0 degrees incidence. The second condition is

included to provide further validation of the grid convergence process for a simpler subsonic case which contains no discontinuities and (possibly) less separation, and thus may be expected to more readily display asymptotically second-order accurate grid convergence.

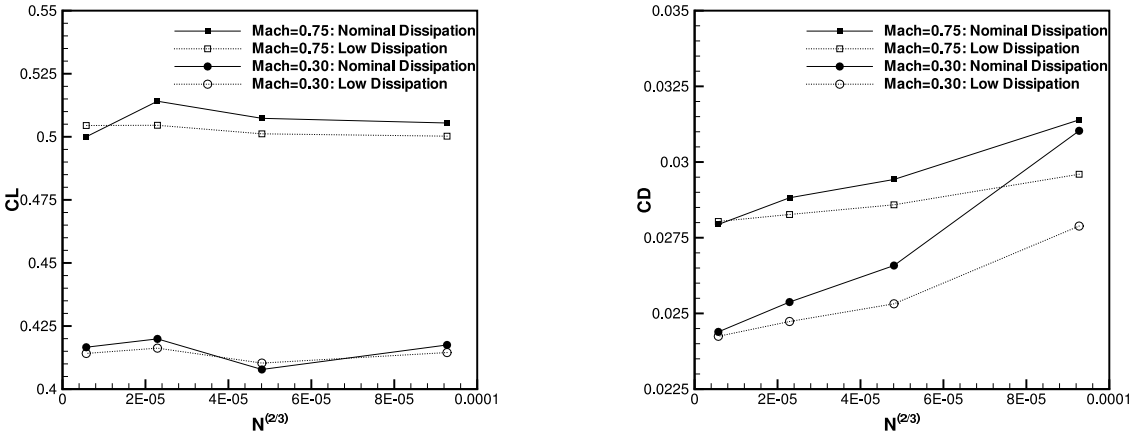

(a) (b)

Figure 5. Comparison of computed lift (a) and drag (b) coefficients versus the number of grid points to the -2/3 power for transonic (M=0.75) and subsonic (M=0.3) cases at 0^o incidence.

Figures 5 and 6 illustrate the computed lift and drag values as a function of the number of grid points to the -2/3 power, for the transonic and subsonic conditions, using nominal and reduced dissipation levels. The drag values in particular appear to be converging asymptotically towards an infinite resolution value with second-order accuracy, as evidenced by the straight line behavior of these plots. Furthermore, the changes in the computed drag coefficient due to the different dissipation levels decreases monotonically with increasing grid resolution, with very small differences remaining for the 72 million point grid. When broken down into pressure and friction drag in Figure 6, the friction drag is seen to be essentially converged, exhibiting little sensitivity to dissipation and grid resolution levels. The computed lift coefficient displays a slightly more erratic behavior, including non-monotone behavior for both the transonic and subsonic cases, although the lower dissipation values are more monotone, and the sensitivity to dissipation is reduced as well on high resolution meshes. For this family of grids(1M, 3M, 9M, and 72M points), the solution thus appears to be converging towards an infinite resolution value.

However, when the same cases are computed on the grid of 65M points, the obtained solution values are substantially different than any of the values obtained on any of the other grids, as shown in Figures 7 and 8, where the results from the 65M point mesh have been added to the previous plots. Note that it is strictly not valid to plot the results from all five grids on the same $N^{-\frac{2}{3}}$ graph, since the latter grid does not belong to the same family of grids. However, this is done in this case to illustrate the changes in the computed values between the two finest grids. The lift at zero incidence on this latter grid is roughly 10% lower than that obtained on the 72M point grid, representing a much larger variation than seen between any of the other grids, and much larger than any of the computed sensitivities due to dissipation, viscous term formulation, or distance function evaluation. It remains very surprising and unexpected that there could be such a large difference between two solutions computed on such fine grids (65M points vs. 72M points), especially in light of the apparent grid convergence path determined by the original family of grids. The lower lift value

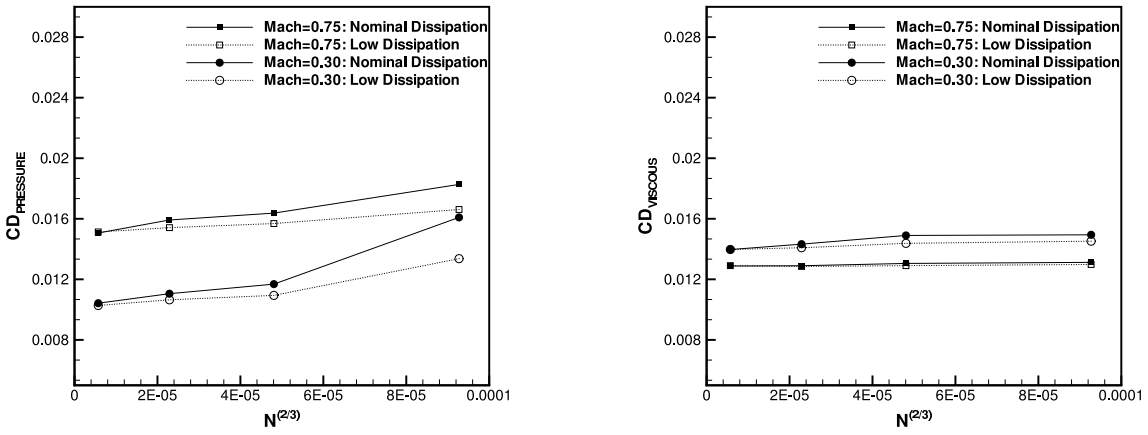

(a) (b)

Figure 6. Comparison of computed pressure drag (a) and friction drag (b) coefficients versus the number of grid points to the -2/3 power for transonic (M=0.75) and subsonic (M=0.3) cases at 0^o incidence.

of the 65M point grid brings the computed lift value much closer to the experimental value of 0.440 at 0^o incidence. However, the computed drag value on this mesh compares less favorably with experiment. In Figure 8(a), the decrease in the drag value is attributable almost entirely to a decrease in the friction drag component, with little observed variation in the pressure drag in going from the 72M point mesh to the 65M point mesh. This is all the more surprising in light of the apparent convergence of the friction drag on the previous set of grids (c.f. Figure 6). It is also worth noting that these trends (lower lift and friction drag) are reproduced for the subsonic M=0.3 case on these grids.

Substantially lower lift values using this same 65M point grid when compared to the previous family of self-similar grids has also been reported in reference,[16] using the FUN3D unstructured flow solver. In fact, the bias between NSU3D and FUN3D results on the same grids reported in[4] (where NSU3D typically computes higher lift values than FUN3D at the same conditions) appears to be preserved on the 65M point grid, providing additional confidence in the validity of both NSU3D and FUN3D computations on this grid. For NSU3D, the lower lift values computed on this grid result in much better agreement with experimental values as shown in Figure 8(b), while for FUN3D, the agreement with experiment is slightly worse, as the amount of separated flow is overpredicted in this case. However, it would be premature to qualify one solution as more accurate than the other at this stage, without a complete grid refinement study and an investigation into the causes for the differences attributable to the use of this particular grid.

In Table 4, the force coefficients and incidence for the specified workshop case of Mach=0.75, C_L=0.5 (as opposed to the fixed incidence 0^o case discussed previously) computed on the 65M point grid are compared with those computed on other meshes. The drag is approximately 19 counts lower than the experimental value, although the incidence and pitching moment are close to the experimental values. These computations are all performed in the fully turbulent mode, and the effects of transition on the drag values for fine grid resolutions remains to be investigated. While the specification of transition trips in the computations were found to further decrease the friction drag in previous computations on coarser grids, the effect of transition on the extent of the trailing edge separation region on the 65M point mesh results remains unknown. Note that while the pressure drag changes little between the constant incidence comparison of results on the fine

grids (c.f. Figure 8(a)), it changes substantially when comparing constant lift conditions between the two grids, due to the different incidences used in these computations.

Table 4. Computed Lift and Drag Coefficients at Mach=0.75, C_L=0.5, on various fine grids.

Grid Size	Incidence	C_L	C_D	C_{DP}	C_{DV}	C_M
65M pts	0.4705	0.5013	0.0276	0.0172	0.0104	-0.1188
72M pts	0.0	0.5045	0.0280	0.0151	0.0129	-0.1481
9M pts	-0.1280	0.4989	0.0282	0.0152	0.0129	-0.1518
Experiment	0.52	0.5000	0.0295	–	–	-0.1211

Results over a range of incidences ($\alpha = 0.0^o, 0.4705^o, 0.827^o, 1.23^o$) have been obtained using the 65M point grid, and are plotted in Figures 8(b), 9(a) and 9(b). The lift versus incidence plot of Figure 8(b) reveals much better agreement with experiment on the 65M point grid compared to all the results on the family of grids derived from the workshop grids. The drag polar plot of Figure 9(a) shows agreement similar to that obtained on the finer workshop grids, although the drag is somewhat lower, mainly due to the friction drag component. The pitching moment values predicted on the 65M point mesh are in much better agreement with experimental values, as shown in Figure 9(b). This is reflected in the surface pressure profiles, which are compared between the 65M point and the 72M point meshes with experimental values for the Mach=0.75 and fixed $C_L = 0.5$ condition in Figure 10 at various spanwise stations. The agreement of the 65M point mesh results with experiment is much improved particularly at the inboard stations, with larger discrepancies remaining at the most outboard stations. The better agreement of lift, moment, and pressure distributions with experimental values for the 65M point mesh is attributed to an increased extent of trailing edge separation along the span of the wing. Since the 72M point and 65M point grids have been designed with similar surface resolutions, it is thus surprising to see such large discrepancies in the solutions for these two grids. In spite of the fact that the 72M point grid includes a finer chordwise resolution of the blunt trailing edge, one may speculate that the use of anisotropic cells in these regions results in the prediction of smaller trailing edge separation regions, which produces substantially higher lift, when integrated along the span of the wing. However, a reliable determination of the causes of these effects can only be obtained through further study.

VII. Conclusions

The current study illustrates the potential for obtaining substantially different solutions on grids of different topologies, even at very fine resolutions, and even in the presence of encouraging grid convergence behavior. This observation, combined with the relatively small sensitivities to other modeling errors such as dissipation levels, viscous term discretization and distance function calculation, reinforces the notion that discretization errors are still the dominant errors in most aerodynamic simulations. Certainly these issues are exacerbated for sensitive off-design conditions such as the current problem involving substantial amounts of flow separation. However, the development of improved turbulence and transition models may well be futile before a better understanding of the discretization errors is achieved. Thorough grid convergence studies using relatively fine meshes are required for acquiring a better understanding and quantification of simulation errors. The availability of state-of-the-art computing facilities has an enormous impact on our ability to advance the state-of-the-art of aerodynamic calculations by making possible the required high-resolution calculations such as those demonstrated in this paper.

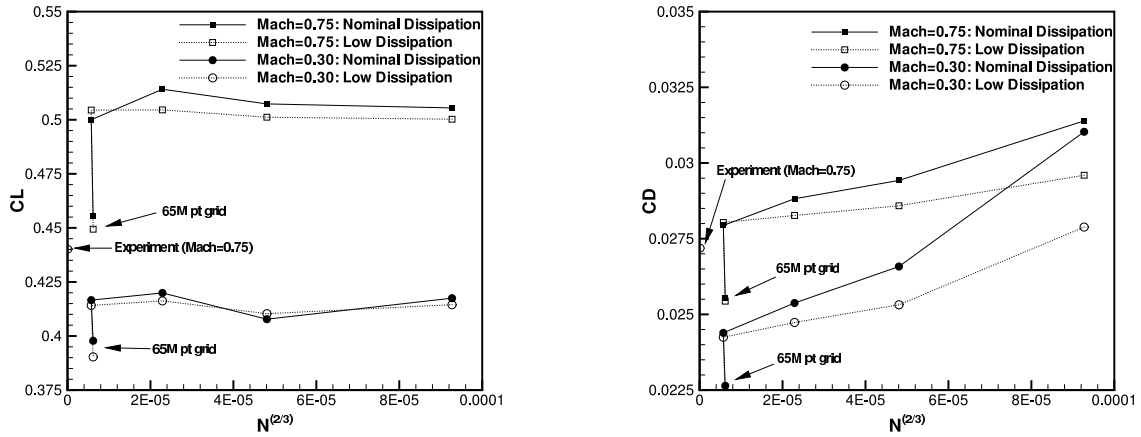

(a) (b)

Figure 7. Comparison of computed lift (a) and drag (b) coefficients versus the number of grid points to the -2/3 power for transonic (M=0.75) and subsonic (M=0.3) cases at 0^o incidence including results computed on the 65 million point grid.

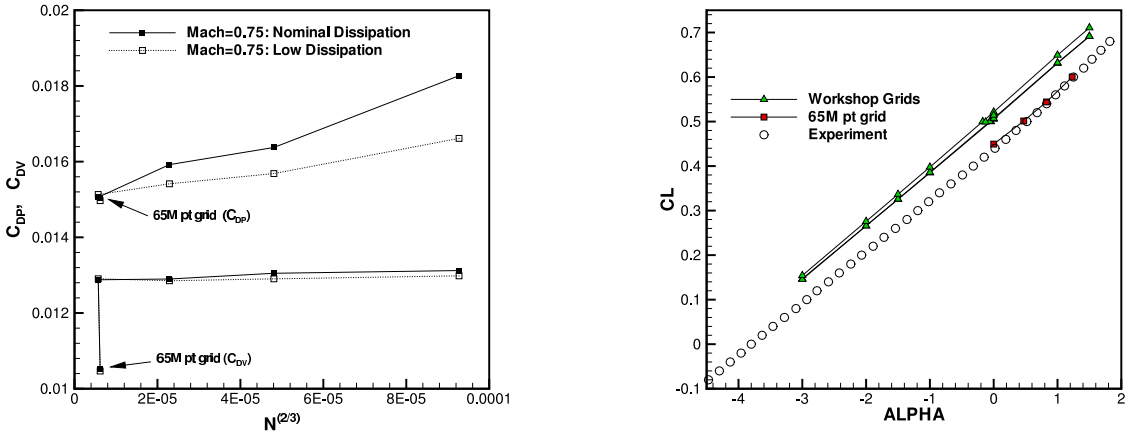

(a) (b)

Figure 8. (a): Variation of computed pressure and viscous drag coefficients on different grids including 65 million point grid for Mach=0.75, 0^o incidence case. (b): Comparison of lift coefficient versus incidence computed on workshop grids and 65 million point grid versus experimental values.

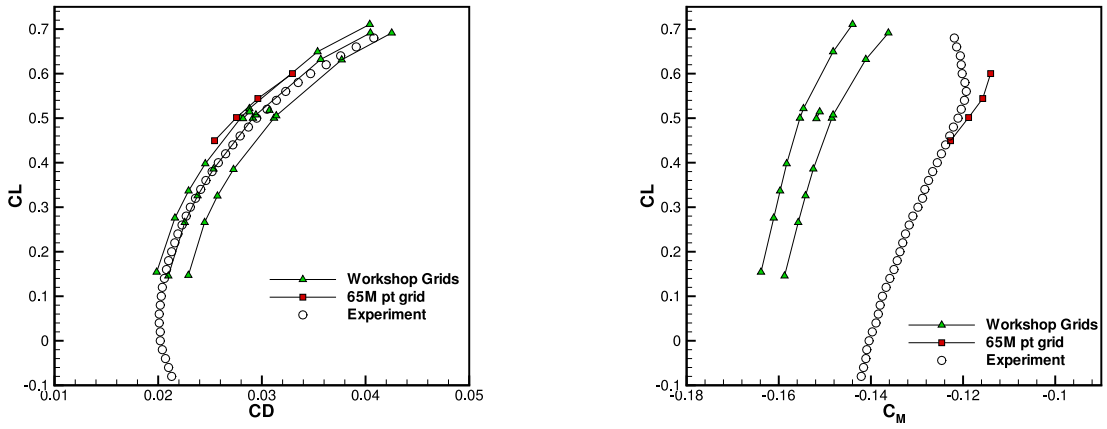

(a) (b)

Figure 9. Comparison of computed drag polar (a) and moment coefficients (b) using workshop grids and 65 million point grid versus experimental values.

VIII. Acknowledgments

The 65M point grid used in this work as generated by S. Pirzadeh at NASA Langley and made available to the author. Zhi Yang of the University of Wyoming performed the implementation of the Eikonal and Poisson equation based distance function routines, and provided the computational results. The computer time made available by the NAS division of NASA was instrumental in the execution of this study, particularly the computations on very fine meshes. Special thanks are due for the allocation of dedicated time on the 2048 cpu cluster at NAS.

References

[1]Levy, D. W., Zickuhr, T., Vassberg, J., Agrawal, S., Wahls, R. A., Pirzadeh, S., and Hemsch, M. J., "Summary of Data from the First AIAA CFD Drag Prediction Workshop," AIAA Paper 2002-0841.

[2]Laflin, K., Brodersen, O., Rakowitz, M., Vassberg, J., Wahls, R., and Morrison, J., "Summary of Data from the Second AIAA CFD Drag Prediction Workshop," AIAA Paper 2004-0555.

[3]Lee-Rausch, E. M., Buning, P. B., Mavriplis, D. J., Morrison, J. H., Park, M. A., Rivers, S. M., and Rumsey, C. L., "CFD Sensitivity Analysis of a Drag Prediction Workshop Wing/Body Transport Configuration," AIAA Paper 2003-3400.

[4]Lee-Rausch, E. M., Frink, N. T., Mavriplis, D. J., Rausch, R. D., and Milholen, W. E., "Transonic Drag Prediction on a DLR-F6 Transport Configuration using Unstructured Grid Solvers," AIAA Paper 2004-0554.

[5]Brodersen, O. and Sturmer, A., "Drag Prediction of Engine-Airframe Interference Effects using Unstructured Navier-Stokes Calculations," AIAA Paper 2001-2414.

[6]Mavriplis, D. J. and Levy, D. W., "Transonic Drag Prediction using an Unstructured Multigrid Solver," AIAA-Paper 2002-838.

[7]Mavriplis, D. J., "Aerodynamic Drag Prediction Using Unstructured Mesh Solvers," *CFD-Based Drag Prediction and Reduction, eds. H. Deconoinck, K. Sermus and C. van Dam, VKI Lecture Series 2003-02, von Karman Institute for Fluid Dynamics, Rhode St-Genese, Belgium*, March 2003.

[8]Mavriplis, D. J. and Venkatakrishnan, V., "A Unified Multigrid Solver for the Navier-Stokes Equations on Mixed Element Meshes," *International Journal for Computational Fluid Dynamics*, Vol. 8, 1997, pp. 247–263.

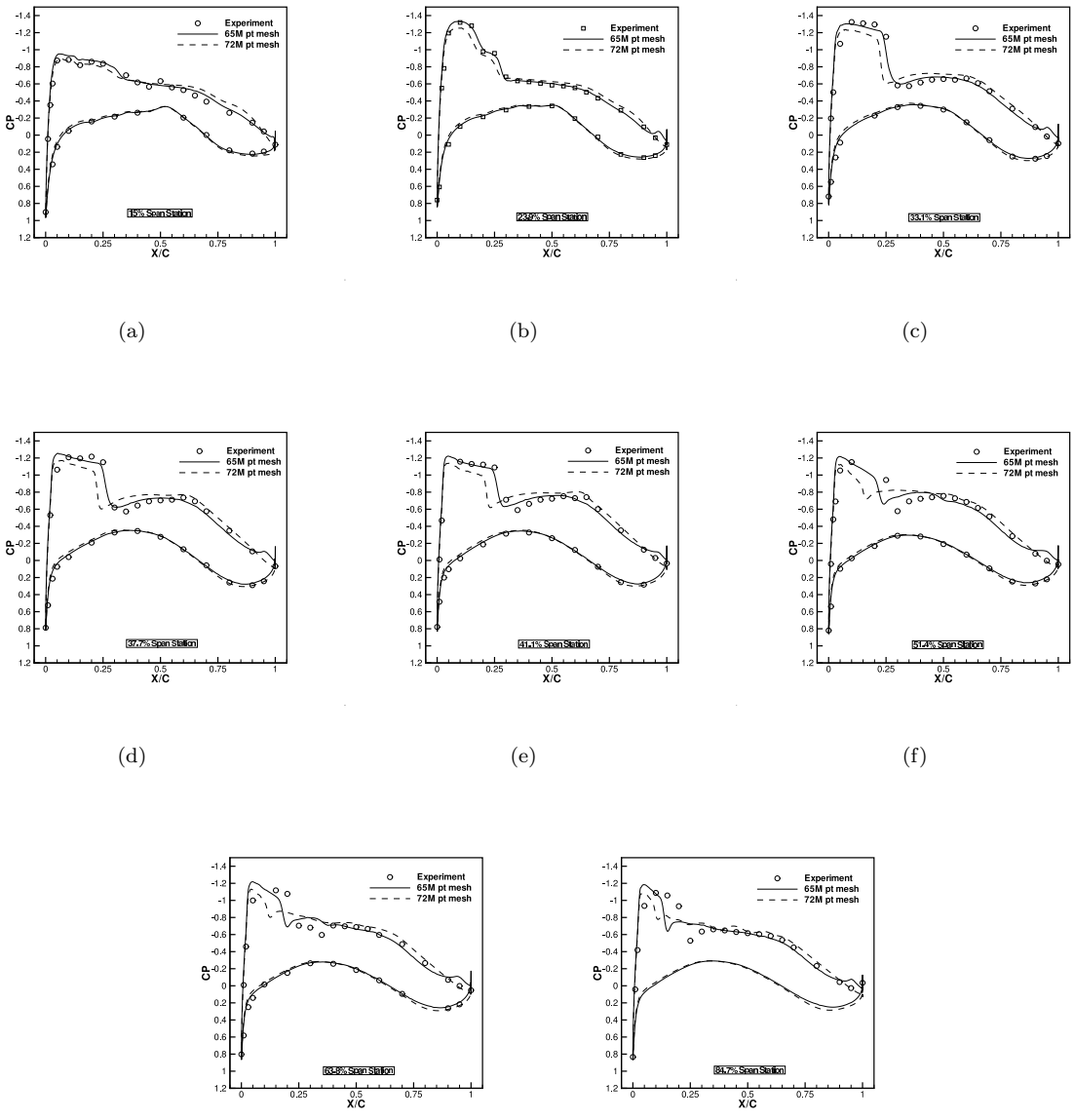

Figure 10. Comparison of computed surface pressure coefficients on 65 million point grid and 72 million point grid versus experimental values for Mach=0.75 and C_L=0.5 case.

[9]Mavriplis, D. J., "Multigrid Strategies for Viscous Flow Solvers on Anisotropic Unstructured Meshes," *Journal of Computational Physics*, Vol. 145, No. 1, Sept. 1998, pp. 141–165.

[10]Mavriplis, D. J. and Pirzadeh, S., "Large-Scale Parallel Unstructured Mesh Computations for 3D High-Lift Analysis," *AIAA Journal of Aircraft*, Vol. 36, No. 6, Dec. 1999, pp. 987–998.

[11]Pirzadeh, S., "Three-Dimensional Unstructured Viscous Grids by the Advancing-Layers Method," *AIAA Journal*, Vol. 34, No. 1, 1996, pp. 43–49.

[12]"Second AIAA Drag Prediction Workshop. Orlando, FL," http://aaac.larc.nasa.gov/tsab/cfdlarc/aiaa-dpw.

[13]Spalart, P. R. and Allmaras, S. R., "A One-equation Turbulence Model for Aerodynamic Flows," *La Recherche Aérospatiale*, Vol. 1, 1994, pp. 5–21.

[14]Sethian, J. and Vladimirsky, A., "Fast methods for the Eikonal and related Hamilton- Jacobi equations on unstructured meshes," *Applied Mathematics*, Vol. 97, No. 11, 2000, pp. 5699–5703.

[15]Tucker, P. G., Rumsey, C. L., Spalart, P. R., Bartels, R. E., and Biedron, R. T., "Computations of Wall Distances Based on Differential Equations," *AIAA Journal*, Vol. 43, No. 3, 2005, pp. 539–549.

[16]Lee-Rausch, E. M., Park, M., Nielsen, E., Jones, W., and Hammond, D., "Parallel Adjoint-Based Error Estimation and Anisotropic Grid Adaptation for Three-Dimensional Aerospace Applications," AIAA Paper 2005-4842.